Technion
Israel Institute of Technology

Faculty of Aerospace Engineering
Research Project 1 (085851)

Research Project Final Report

Phrasing testing methodology for quantifying the influence of plasma actuator on subsonic flow separation

Matar M. Rosen

Advisors:
Anton Ronis
Asst. Professor Igal Kronhaus

September 23, 2019

This report serves as preliminary research and design for a study of active flow control via plasma actuation. The variables that could influence the experiment are discussed and a choice of parameters is made and explained. The choice of wind-tunnel model- backward facing step and it's dimensions is reasoned and presented along with the CAD design. The different constraints, requirement and variables are taken into account, the compromises discussed and finally the suggested experimental process and measuremnt techniques are presented.

Contents

Nomenclature

Abbreviations

AFC	Active Flow Control
BFS	Backward Facing Step
BL	Boundary Layer
CAA	Cathodic Arc Actuator
CAJ	Cathodic Arc Jet
IGBT	Insulated Gate Bipolar Transistor
LCS	Large Coherent Structures
LE	Leading Edge
ns-DBD	nano second Dielectric Barrier Discharge
PPU	Power Processing Unit
VG	Vortex Generator

Nomenclature

δ	Boundary layer thickness
ν	Kinematic viscosity
$\overline{x}$	Normalized length/location of interest ($= x/h$)
ρ_∞	Freestream density
τ_w	Wall shear stress
θ	Momentum boundary layer thickness
AR	Aspect Ratio ($= \text{span}^2/\text{reference surface}$)
C_μ	Momentum coefficient
C_f	Skin friction coefficient
ER	Expansion Ratio
F^+_{hu}	Reduced frequency based on step height and CAJ velocity
$F^+_{X_bU}$	Reduced frequency based on bubble length and freestream velocity
$F^+_{X_bu}$	Reduced frequency based on bubble length and CAJ velocity
f_{ac}	Actuation frequency
f_{sh}	Vortex shedding frequency
H	Height of test section above tread
h	Step height
L	Tread length
l_{caj}	CAJ length
n	Number of pulses per packet
Re	Reynolds number ($= U \cdot L/\nu$)
Re_θ	Reynolds number based on momentum thickness ans freestream velocity
Re_{hU}	Reynolds number based on step height and freestream velocity
Re_{LU}	Reynolds number based on tread length and freestream velocity
St	Strouhal number ($= f \cdot L/U$)
St_θ	Strouhal number based on momentum thickness θ
St_h	Strouhal number based on step height
T_h	Test section height
T_L	Test section length
TI	Turbulent Intensity
U_∞	freestream velocity
u_τ	Shear velocity
u_{caj}	CAJ velocity
V_p	Vertical position of the model in the test section
W	Test section/Model span
X_b	Separation bubble length

1 Introduction

1.1 Research Objective

The objective of this report is to prepare the groundwork for an experiment that will asses the performance of a Cathodic Arc Actuator (CAA) as a subsonic flow control actuator. This report details four measures taken to answer the research question: literary review and background of flow separation and flow control actuators and specifically plasma actuators, assembly of experimental parameters relevant to flow separation due to backward facing step configuration, tuning the experimental parameters with the characteristics of the cathodic are jet, and formulation of an experimental process that quantifies the influence of the CAA on the separation region of a backward facing step model subjected to subsonic flow.

1.2 Background

Flow separation is the detachment of flow from a solid surface. Wall friction and adverse pressure gradient reduce the momentum and kinetic energy of fluid particles in the boundary layer (BL), until eventually their motion stops, the streamlines no longer follow the wall and the flow is separated [1]. Flow separation occurs in engines, vehicles (cars, boats), around buildings, and in aerospace applications [2]. Several notable drawbacks of separated flow are acoustic noise problems [3], drag increase, lift losses [4], instabilities, and more. Often postponing flow separation and avoiding mentioned losses is desired, although in some cases provoking the boundary layer separation is advantageous [1]. Consequently, separation control is of interest in many applications.

To avoid aerodynamic losses associated with flow separation one could constrain flight to certain conditions (flight envelope). Alternatively one could design a device to interact with the separated flow to try and control its properties, i.e. separation control. Separation control is part of flow control, which is a subfield of fluid mechanics that deals with manipulating the behavior of flows. The term applies to any actions or interventions that cause change that otherwise would not occur in naturally developing flow.

Flow control methods are often divided into categories, for instance: according to their energy expenditure, into passive and active control methods.

1.2.1 Passive Flow Control

Refers to methods that manipulate the flow by structural means, with no external power acting on the flow. The main mechanism through which passive devices assert control over the flow is through turbulence augmentation methods that energize and improve the flow's resistance to separation [1]. Some disadvantages of passive control devices are the constant addition of drag, and low control authority for low local velocities, e.g. in the region of separated flow.

Vortex Generator (VG) is a common example of such a device dating back to the 1940's [5]. These are small airfoils installed normal to the surface. They overturn the flow near the wall so that energetic fluid particles are lowered to the surface and enrich the boundary layer [1]. They are simple and effective but have the disadvantage of adding significant parasitic drag that impairs platform performance.

1.2.2 Active Flow Control

In 1904 Ludwig Prandtl introduced the concept of the boundary layer, the phenomenon of separation and described several experiments in which steady active control could be used to control the boundary layer [1]. Active Flow Control (AFC) can be divided to steady control (classic), and periodic active control.

Classic AFC Steady blowing and or suction have been shown to improve lift and reduce drag in aerodynamic platforms [4]. Steady blowing introduces momentum to the part of the BL that is lacking, thus postponing separation [6]. Steady suction removes slow fluid particles while bringing energetic ones closer to

the surface thus enhancing the overall momentum in the BL and postponing separation [6]. The implementation of these ideas turned inefficient due to increased weight and complex design requirements that overcame the performance gain, if any, obtained using them.

Periodic AFC These type of methods excite flow instabilities by manipulating Large Coherent Structures (LCS) via periodic perturbations [4, 7]. LCS transport momentum about the flow domain and act as the main mechanism for diffusing momentum.

Due to the broad range of means for generating periodic perturbations, there are many actuators in existence that interact with the flow in various means. One way of classifying actuators is according to their

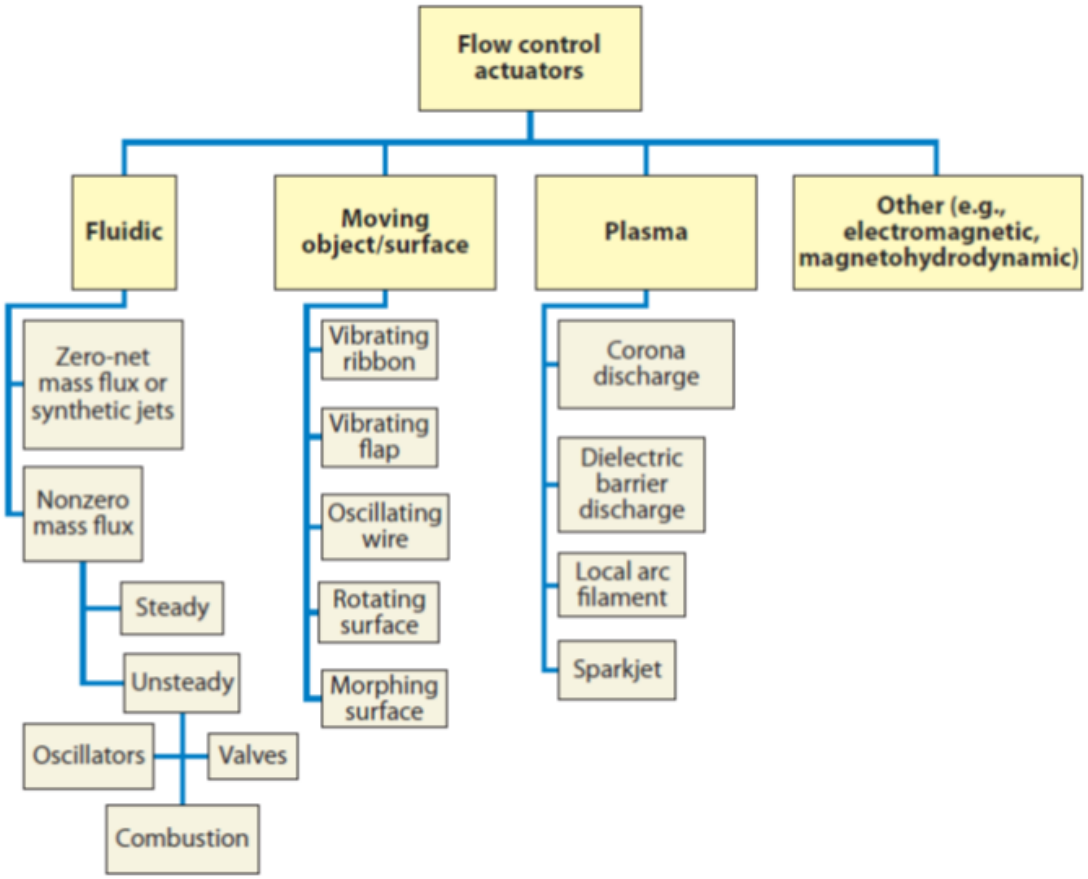

Figure 1: A diagram of different types of flow actuators, taken from Cattafesta et al. [8]

function, see for example Fig.1. Fluidic actuators interact with the flow through injection or suction of fluid particles. These include synthetic jets, through which the net mass flux is zero, and non-zero mass flux jets [9]; moving object/surfaces that interact with the local flow field [10,11]; plasma actuators, characterized by no moving parts, low mass and fast time response [12].

Plasma actuators can be further divided into thermal and non-thermal actuation. Thermal plasma actuators, such as the Localized Arc Filament Plasma Actuators (LAFPA), excite the flow by localized heating that creates pressure perturbations [13]. Schematically shown in Fig. 2a, the LAFPA was shown to enhance mixing in high-speed and Reynolds number jet flows. [14]. The SparkJet (see Fig. 2b), is another thermal plasma actuator which operates by rapidly heating trapped air inside a close cavity by forming a high current

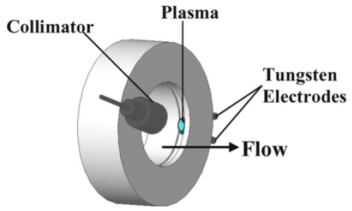

(a) Schematic of a nozzle extension, LAFPA and fibre optic link collimator used for plasma temperature measurements. Taken from Utkin et al. [14]

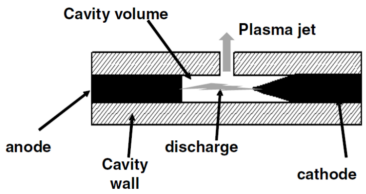

(b) Schematic of SparkJet actuator. Taken from Narayanaswamy et al. [15]

arc, and then expelling the high-pressure high-temperature gas through a small orifice towards the unperturbed flow [15]. Similarly to LAFPA, this actuator has a wide bandwidth range ($\sim$ kHz) and additionally a high injection velocity ($\sim$ 300 m/s) [15].

Nano-second pulsed dielectric barrier discharge plasma actuator (ns-DBD) is another thermal plasma actuator. Both Correale and Esfahani et al. [16, 17] demonstrated the control authority of these actuators by effecting the reattachment location of a separated flow. A schematic of the ns-DBD can be observed at Fig. 3a.

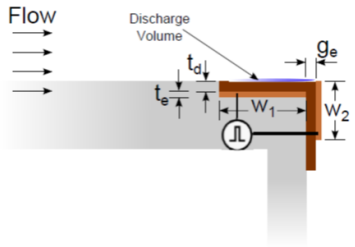

(a) Schematic drawing of ns-DBD plasma actuator side view. Dimensions of plasma actuator out of scale for clarity. Location of discharge volume indicated with respect to the step and electrodes position. from: Flow control over a backward facing step by ns-DBD [16]

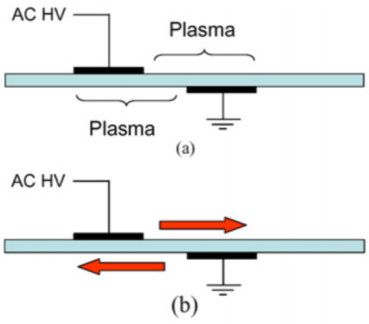

(b) Schematic side view of a single DBD actuator, (a) area of plasma, (b) electric wind direction. From: Air Flow Control By Non-Thermal Plasma Actuators [12]

Non-thermal plasma actuators excite the flow using discharge-induced electric wind [12]. Usually with flush mounted electrodes that accelerate the flow tangential to the wall. An example is the Alternating Current Dielectric Barrier Discharge (AC-DBD) plasma actuator [12]. The actuator is composed of two planar electrodes at two sides of a dielectric barrier, one electrode is connected to an AC high voltage input, and the other is grounded, see Fig. 3b. Ionized air is generated periodically in correspondence with the frequency of actuation.

SHORT BACKGROUND on the CAA (relate to VAT and what is the CAJ). An electric arc is an electrical discharge between two electrodes, characterized by high current and low voltage. A cathodic arc is a type of electric arc that is maintained through the production of highly ionized plasma by a combination of joule heating and ion bombardment heating that maintain the conditions required for electron emission and vaporization of cathode material. When generated in vacuum cathodic arcs produce fast plasma plumes. Cathodic arcs in atmospheric pressure gas produce fast jets of gas, termed cathodic arc jets [18]. The cathodic arc actuator (CAA) is a plasma actuator device developed in the Aerospace Plasma Laboratory (APL) in the Technion.

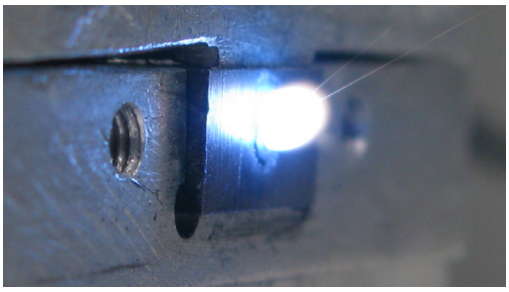

(a) CAJ photo- from ??

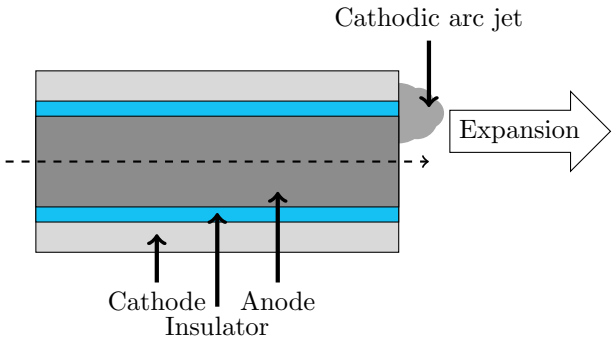

(b) Schematic of the CAA

1.3 Cathodic Arc Actuator

The actuator is made from a stainless steel cathode, a tungsten anode and an alumina insulator separating the two electrodes [18]. The actuator is cylindrical (as seen in Fig.4b) and the jet is in the direction of the symmetry axis. The ignition of the arc requires high voltage ($\sim$ 1.4 kV [18]) and afterwards high current ($\sim$ 120 A) supply, therefore a regular power source is not sufficient and a power processing unit (PPU) is used to power the CAA.

1.3.1 Power Processing Unit

The PPU is a modified version of an inductive power processing unit, and is composed of two 1.7 kV insulated-gate bipolar transistors (IGBT) responsible for switching between charging the coil, and igniting the arc [19] (S_1), and for shutting off the discharge (S_2). The circuit logic is governed by an on-board microprocessor. The schematic of the PPU circuit and the different stages of work are illustrated in Fig.5b. At stages (a)

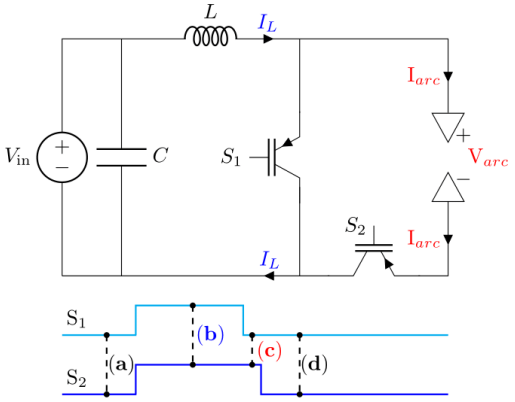

(a) Schematic of the PPU

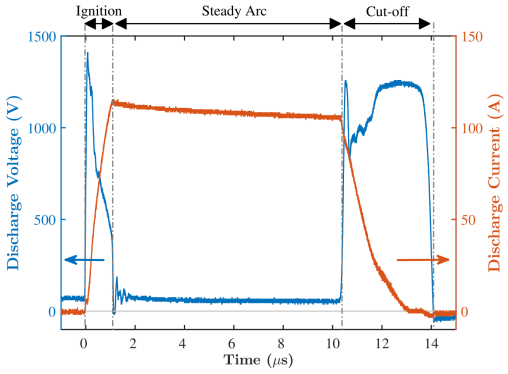

(b) I-V time history for a discharge time of $\approx 10\ \mu s$

Figure 5: Taken from [19, 20]

and (d) both IGBTs (S_1 and S_2) are open, the system is disconnected and the potential difference across the electrodes is of V_{in}. At stage (b) the IGBTs are closed, the current I_L charges the coil. At stage (c), opening S_1 after the coil is charged, causes a sudden change in current that in turn adds the coil's energy to the original V_{in}, this voltage peak across the electrodes ignites an arc. The arc current I_{arc} is driven between the electrodes and is characterized by a relatively constant potential difference V_{arc}, opening S_2 triggers cut-off of the arc current and returns the circuit to the initial state (a).

Fig.5a presents a typical time history of the discharge voltage and current over a $\sim 10\ \mu s$ duration. The discharge time can be divided into three stages that are visualised on top of the figure: ignition- after S_1 has been opened, the potential difference between the electrodes is the breakdown voltage of ~ 1.4 kV and the current has a peak of ~ 120 A. During the steady arc stage the discharge voltage drops to a relatively constant value of ~ 30 V and the current slowly drops from its peak value. At the final stage of cut-off- after S_2 has been opened and disconnects the circuit, the arc current drops to zero that triggers a second voltage peak from the residual energy stored in the coil.

1.4 Backward-Facing Step

The backward-facing step (BFS) is one of the simpler and most common aerodynamic models for flow separation. This model is popular due to many reasons, some of which are: fixed separation point; no side effects due to curvature, uncertain freestream flow conditions, and three dimensional flow.

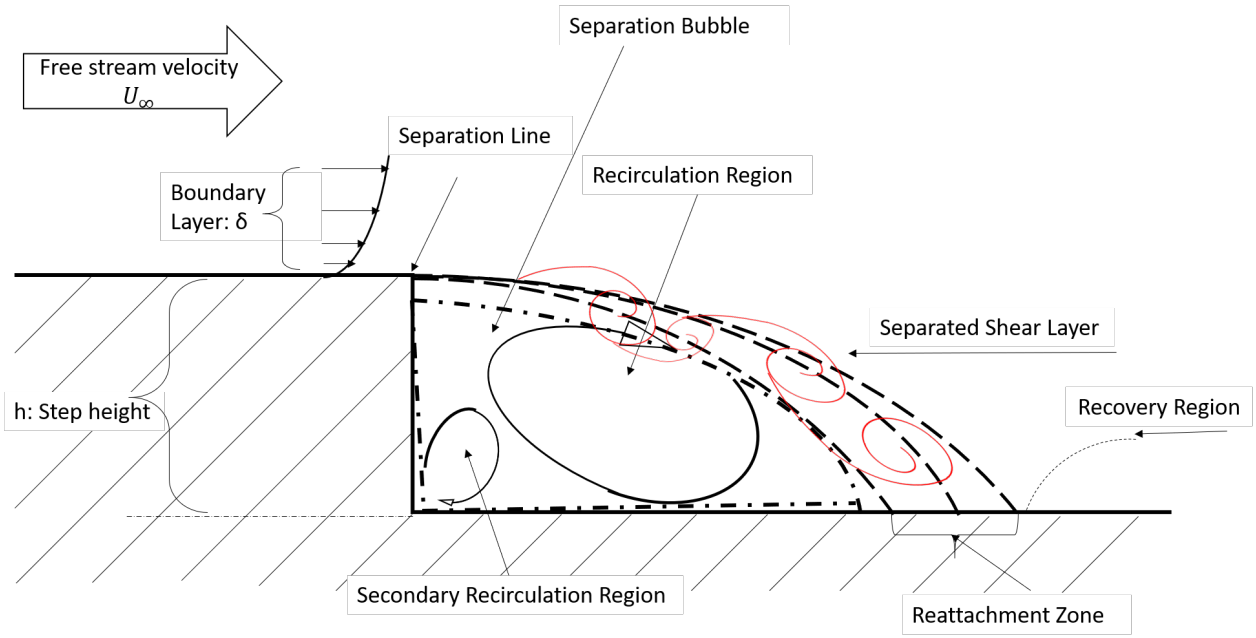

Figure 6: Schematic of the flow regions about a backward facing step model

The BFS model is subjected to a uniform freestream velocity (U_∞), with a separation point anchored by a step of height h. The resultant flow field can be divided into four regions as visualized in Fig.6: separated shear layer, re-circulation and secondary re-circulation, reattachment and recovery regions [2].

1.5 Experimental Parameters

The experimental parameters in backward-facing subsonic flows include [2, 4]: Freestream flow conditions (U_∞ - velocity), Step geometry (h step height, ER Expansion Ratio - height before and after the step), and others. Specifically, the experimental parameters covered are:

1. U_∞ - Freestream velocity.
2. L - Tread length (length before separation).
3. δ - boundary layer thickness.

4. ν - Kinematic viscosity.
5. $Re = U_\infty L/\nu$ - Reynolds number.
6. $\frac{x}{h}$ - normalized scale.
7. f_{sh},f_{ac} - vortex shedding and actuation frequencies.
8. $St = f \cdot L/U$ - Strouhal number.
9. Cathodic Arc Jet (CAJ) characteristics:
   (a) u_{CAJ} - CAJ mean velocity $\sim$ several hundreds of m/s.
   (b) l_{CAJ} - CAJ length: ~ 1.5 mm.
   (c) n - number of pulses in a packet, for the baseline measurement $n = 1$.
10. Leading edge geometry and others (we used a geometry that worked for a similar case)

2 Methods

This section presents the attempt to minimize the variables for the experiment. The previous section (1.5), introduced the possible parameters for the experiment. To reduce the amount of independent parameters, the relations between parameters and the values that proved to be in the range of values for actuators that are similar to the CAA were considered.

The relations are presented in Table 1, and in the following explanations. In the table, each row and column correspond with a specific parameter, and where each cell refers to the relation between the matching parameters. Non-blank values on the table diagonal represent valued constraints.

	h	T_h	H	ER	T_L	L	W	U_∞	X_b	f	u_{caj}	l_{caj}	δ	Re_{hU}	Re_{LU}	St_h	F^+_{hu}	$F^+_{X_bU}$	$F^+_{X_bu}$	C_μ
h	-	II,III	II	III	0	0	0	VI,XII	I	XII	XIII,XIV	VIII	0	VI	VII	XII	XIII	0	0	0
T_h		II	II	III	0	0	0	0	I	0	0	0	0	0	0	0	0	0	0	0
H			-	III	0	0	0	0	0	0	0	0	0	0	0	0	0	0	0	0
ER				-	0	0	0	0	I	0	0	0	0	0	0	0	0	0	0	0
T_L					IV	IV	0	0	0	0	0	0	0	0	0	0	0	0	0	0
L						-	0	VII	0	0	0	IX	IX	0	VII	0	0	0	0	XVI
W							V	0	0	I	0	0	0	0	0	0	0	0	0	0
U_∞								-	I,XIV	XII	X	0	IX	VI	VII	XII	0	XV	0	0
X_b									-	XIV,XV	0	0	0	0	0	0	0	XV	XIV	0
f										-	XIII,XIV	0	0	0	0	XII	XIII	XV	XIV	XVI
u_{caj}											-	XI	0	0	0	0	XIII	0	XIV	XVI
l_{caj}												-	IX	0	0	0	0	0	0	XVI
δ													-	0	0	IX	0	0	0	0
Re_{hU}														-	0	0	0	0	0	0
Re_{LU}															-	0	0	0	0	0
F^+_{hU}																-	0	0	0	0
F^+_{hu}																	-	0	0	0
$F^+_{X_bU}$																		-	0	0
$F^+_{X_bu}$																			-	0
C_μ																				-

Table 1: Experimental parameters matrix

The relation between the parameters marked with (0) refer to parameters that weren't considered due to either being unrelated, or having an unclear relationship.

Non-dimensional formulation:

(I) Chen et al. [2], collected parameters that control the separation bubble length, in the following implicit equation:

$$\frac{X_b}{h} = f\left(AR, ER, Re_\theta, Re_{hU} \cdot \frac{\delta}{h}, TI, \frac{\partial p}{\partial x}\right) \tag{1}$$

Where AR is the aspect ratio, ER is the expansion ratio, TI is the Turbulent Intensity, a property of the wind tunnel, on which we have no control, thus it is not a variable in planning the experiment (but should be considered when analysing the results). Re_θ and Re_{hU} are Reynolds numbers, further explained below, δ is the BL thickness, h is the rise height of the model, and $\frac{\partial p}{\partial x}$ is the pressure gradient.

Geometrical constraints:

- (II) The total height of the test section is $T_h = 0.5\ [m]$, and it includes

  $$T_h = h + H + V_p = 0.5\ [m], \tag{2}$$

  where h is the step height, H is the vertical distance between the tread and the top of the test section, V_p is the vertical position of the model in the test section.

- (III) The expansion ratio of the BFS model

  $$ER = \frac{h + H}{H}. \tag{3}$$

- (IV) The total length of the test section is $T_L = 1.35\ [m]$, it limits the tread length, and defines the space available for flow diagnostics.

- (V) The span of the test section is $W = 0.5\ [m]$, this limits the span of the BFS model.

Reynolds numbers:

- (VI) Reynolds number based on step height and freestream velocity:

  $$Re_{hU} = \frac{h \cdot U}{\nu}, \tag{4}$$

  (ν is the kinematic viscosity). This form of the Reynolds number will be used in comparison with other published findings.

- (VII) Reynolds number based on tread length and freestream velocity:

  $$Re_{LU} = \frac{L \cdot U}{\nu} \tag{5}$$

  This Reynolds number was used to estimate the boundary layer thickness at the step rise, where the actuator was located, to estimate the CAJ length in wall units. This calculation can be seen in appendix A.

- Reynolds number based on incoming flow momentum boundary layer thickness and velocity:

  $$Re_\theta = \frac{\theta \cdot U_\infty}{\nu}, \tag{6}$$

  where θ is the momentum boundary layer thickness. This Reynolds number is also very common in other works in the subject of BFS flow control, but due to the difficulty of assessing θ in advance it is not helpful in planning the experiment. Although we make no use of it in this work, this form of the Reynolds number would be a part of the post-process of the experiment.

CAA and CAJ properties:

- (VIII) The separation bubble's dimensions are effected by the step height. To avoid bursting the bubble, the CAJ length should not be much greater than the step height, but for the CAA to have influence over the reattachment location, the CAJ length should not be much smaller than the step height.
- (IX) The actuator should have influence over as many LCS in the BL, since there is no well accepted rule for which eddies will have the desired effect for separation control. Wanting to reach most of the boundary layer's energetic coherent structures which can be found in the viscous sublayer region [1]. The BL thickness (δ) depends on $Re_{x=L}$ (discussed in the Appendix A).
- (X) The freestream velocity should fit the optimal conditions for the experiment, that would be determined according to the CAA properties.
- (XI) inter relations of the CAA parameters: the velocity and length of the CAJ are related, but that is not in the scope of this work.

Flow control parameters:
Strouhal numbers and reduced frequencies[1], can help compare the experimental conditions in this work to other experiments and determine the best actuation frequency to test. Here we consider several forms of reduced frequencies:

- (XII) Strouhal number based on step height:

$$St_h = \frac{f \cdot h}{U} \tag{7}$$

- (XIII) Reduced frequency based on step height and CAJ velocity:

$$F^+_{hu} = \frac{f \cdot h}{u_{caj}} \tag{8}$$

- (XIV) Reduced frequency based on bubble length and CAJ velocity:

$$F^+_{Xbu} = \frac{f \cdot X_b}{u_{caj}} \tag{9}$$

  This would be applicable during the experiment, when the length of the separation bubble will be measured.

- (XV) Reduced frequency based on bubble length and freestream velocity:

$$F^+_{XbU} = \frac{f \cdot X_b}{U} \tag{10}$$

  Similarly to above, this would be applicable during the experiment.

- Strouhal number based on momentum thickness θ:

$$St_\theta = \frac{f \cdot \theta}{U_\infty} \tag{11}$$

  Strouhal number based on momentum thickness is a sensible choice of parameter for flow control, as it relates the perturbation frequency and the momentum thickness – two key factors for flow control authority. According to Hasan [21], an optimum value exists for $St_\theta = 0.012$. This will be tested during the post-process of the results.

[1]Reduced frequency is equivalent to the Strouhal number when the reference velocity is the freestream velocity

Note that the reduced frequencies are either for the actuation frequency or the shedding/natural shedding frequency.
(XVI) Momentum coefficient is a standard measure of relative momentum addition [4]. The momentum coefficient is divided into steady and oscillatory contributions: $C_\mu = (c_\mu, < c_\mu >)$, in our case $c_\mu = 0$ since there is only oscillatory momentum addition. Oscillatory momentum coefficient as defined by Greenblatt et al. [4]:

$$< c_\mu >= \frac{1}{\frac{1}{2}\rho_\infty U_\infty^2 L}\rho_\infty \int_0^\infty u_{caj}^2 dy \tag{12}$$

It will be used to evaluate the control authority of the CAA. Here u_{caj} is the fluctuating component of the CAJ velocity and ρ_∞ is the freestream density.

Further constraints and ranges of possible values were applied by examining current published results dealing with similar plasma actuators installed on a BFS model [2, 16, 17]. The ns-DBD (nano second pulsed Dielectric Barrier Discharge plasma) actuator is one such actuator. Correale [16] investigated optimal actuation frequencies for the ns-DBD actuator in BFS flow, the experimental conditions were: $Re_{hU} = 3600$, and $U_\infty = 5$ $[\frac{m}{sec}]$ they demonstrated improvement of reattachment location. Their actuation frequency was $f_{ac} = 160$ $[Hz]$, and this should be translated to reduced frequency.

Further explanations will be elaborated in the Results and Discussion section below.

3 Results and Discussion

3.1 BFS Model

The model we devised for this experiment is shown in Fig. 7. The CAA was positioned as close to the riser of the step as possible, in two orientations - normal (located at the edge of the tread), and parallel (located at the top of the raiser) to the local flow field. The first orientation introduces perpendicular momentum to the flow, whereas the second orientation will examine the addition of momentum along the flow inside the separated region.

The dimensions of the model are:

- Rise: $h = 10$ mm, that should be enough to enable positioning the CAA in the parallel position, and coincide with the targeted Reynolds number of ≈ 3600 [16] (VI). Furthermore, the rise of the step is in the same scale as the CAJ length, as discussed in (VIII).
- Span: $W = 450$ mm as wide as the test section allows (V), to avoid three dimensional effects.
- (IV) Tread: $L = 150$ mm containing a half ellipse leading edge (LE), and a straight section before the edge (75mm,75mm). The half ellipse LE is meant to attach the flow to the model, and the straight section to allow the BL to stabilize.
- Length downstream of the riser: 500 mm, which should be enough space for the flow to reattach and for placing the diagnostic devices.
- Vertical position - in the middle of the test section: $V_p = 250$ mm
- The resulting expansion ratio is $ER \approx 1.04$, similar to Correale's [16] expansion ratio: $ER = 1.06$.
- The model also includes a trailing edge flap to adjust the stagnation point.

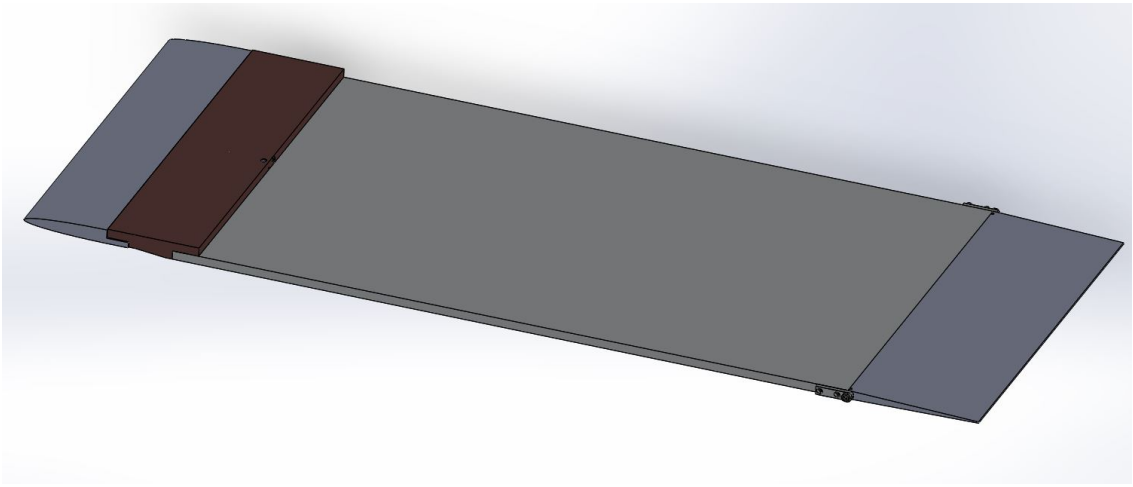

(a) BFS CAD Model

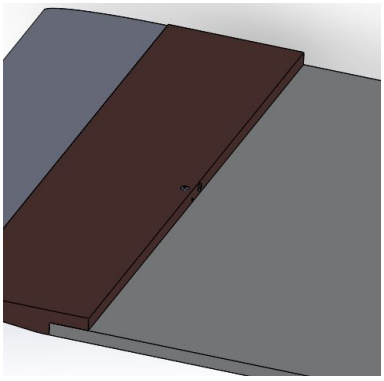

(b) BFS CAD Model zoom

Figure 7: BFS CAD Model

3.2 Experimental Plan

Remembering the initial goal of validating the actuator's effect on the reattachment distance, and since the actuator's main excitation method is through periodic excitation - the first test would be to find the flow's natural shedding frequency.

We suspect that the optimal actuation frequency would be higher then the natural shedding frequency. Correale [16] had shown that the optimal actuation frequency is not the natural frequency of the flow, but the frequency with the highest energy density. According to Hasan [21], it should produce a $St_\theta \approx 0.012$. Therefore, after using a hot wire measurement to find the natural shedding frequency (f_{sh}), the following actuation frequencies will be tested:

$$f_{ac} = 0, f_{sh} - 40, f_{sh} - 20, f_{sh}, f_{sh} + 20, f_{sh} + 40, f_{sh} + 60, f_{sh} + 80, f_{sh} + 100$$

These measurements would first be conducted with $Re_h = 3600$ that worked well for ns-DBD [16], since that type of actuation is most similar to ours. This step-height Reynolds number translates to:

$$U_\infty = 10 \ \frac{m}{s}$$

If in that flow velocity the actuator's effect will not be significant, other flow velocities will be tested:

$$U_\infty = 8, 12 \ \frac{m}{s}$$

with the same process for determining the natural shedding frequency and the optimal actuating frequency.

After the optimal actuating frequency is determined, a range of added momentum values (XVI) will be tested. A common method of quantifying the momentum addition [4] is with the momentum coefficient: C_μ. Different momentum coefficients will be tested at the optimal frequency, by changing the number of pulses in the packet:

$$n = 1, 5, 10.$$

In addition, the St_θ would be calculated for the PSD (from the hot wire measurements) and St_h would be calculated for the actuation frequencies. After which compatibility with the theoretical [21] values ($St_\theta = 0.012$ and $0.2 < St_{h,opt} < 0.4$) would be evaluated.

3.3 Diagnostics

This section presents the diagnostic methods [22] that will be used to measure and quantify the experimental results of the proposed methodology.

Oil Flow Visualization

Surface Oil Flow: Provides qualitative information on the flow. Oil drops placed on the model will be carried with the flow and illustrate flow patterns that will help visualize the separation boundary.
Oil Film Interferometry: Quantitative information. Thin oil film applied to the model. The oil responds to aerodynamic shear from the air flow above it. The wall shear stress τ_w is calculated from the temporal oil film thickness measurement [23].

Hot Wire Anemometry

The recorded flow fluctuations are used to calculate vortex shedding frequency. The local velocity profile will be measured at several spatial locations along the BFS.

Surface Tufts

Small strands of string with frayed ends attached to the surface of the model. The direction of the tufts indicates the flow in its region thus marking flow reattachment, recirculation, etc. Also used to visualize the evolution of the separation region.

Smoke

Used to visualize the flow field above the boundary layer. Can detect vortexes and visualize the separation bubble and shear layer.

4 Conclusion

In conclusion, this report provides an overview of a planned experiment for evaluating the control authority of the CAA on a BFS model subjected to subsonic flow. The report includes a background of flow separation theory and of ways to mitigate it. The experimental parameters affecting separated flow of a BFS are analyzed and compared with CAA characteristics and published results. Based on the analysis, an experimental

campaign is designed along the desired BFS model. A set of diagnostics is included as well, to record and quantify the wind tunnel results. These will be used to answer the research objective and to verify the published results.

A Appendix

Wall units

Wall units are non-dimensional units normalized by wall properties. They are commonly used in phenomenon that occur in the boundary layer, such as separation.

Wall units and helpful estimations[2]

Distance from the wall:	y	$[L]$
(mean) Velocity profile:	$u(y)$	$\left[\frac{L}{T}\right]$
Blasius laminar flow: skin-friction estimation:	$C_f = \frac{0.664}{\sqrt{Re_x}}$	[ ]
Shear stress at the wall:	$\tau_w = C_f \cdot \frac{1}{2}\rho_\infty U_\infty^2$	$[\frac{M}{LT^2}]$
Fluid density:	ρ	$[\frac{M}{L^3}]$
Kinematic viscosity:	ν	$[\frac{L^2}{T}]$
Shear velocity:	$u_\tau \triangleq \sqrt{\frac{\tau_w}{\rho}}$	$[\frac{L}{T}]$
$\Downarrow$		
Velocity in wall units	$u^+ = \frac{u(y)}{u_\tau}$	[ ]
Distance normal to a surface in wall units	$y^+ = \frac{u_\tau \cdot y}{\nu}$	[ ]

Boundary Layer Thickness

The following approximations[3] were used to evaluate the limitation to tread length, in order to avoid a boundary layer too high for the actuator.

$$\delta \approx 4.91\frac{x}{\sqrt{Re_x}} \quad ; \text{ for laminar BL} \tag{13}$$

Validation

(Calculation that shows the location of the actuator (at the rise of the step) is indeed at 100 wall units, and inside the BL).

The calculations will assume the kinematic viscosity of air in RT $\nu \approx 15 \cdot 10^{-6}$ $[\frac{m^2}{sec}]$ and that the boundary layer is laminar.

[2] `https://www.cfd-online.com/Wiki/Y_plus_wall_distance_estimation`,`https://en.wikipedia.org/wiki/Skin_friction_drag`

[3] the approximation derived from the Blasius solution to the BL governing equations, taken from Wikipedia

At $x = L = 150$ $[mm]$ the height of the BL can be approximated according to equation (13):

$$\delta_{lam} = 4.91 \frac{0.150\ m}{\sqrt{\underbrace{\frac{0.150\ m\ \cdot 10\ \frac{m}{sec}}{15 \cdot 10^{-6}\ [\frac{m^2}{sec}]}}_{Re_x @ x=L}}} = 4.91 \frac{0.150\ mm}{\sqrt{\frac{15 \cdot 10^5}{15}}} = \frac{0.7365\ m}{\sqrt{10^5}} = 2.329 \cdot 10^{-3} > 1.5\ mm$$

In conclusion, in both laminar and turbulent cases, the targeted $y^+ = 100 = l_{caj}$ is in the BL.

Physical distance above the wall

Using the wall units estimations:

$$\begin{aligned} Re_x = \frac{U_\infty L}{\nu} &= \frac{10 \cdot 0.15}{15 \cdot 10^{-6}} = 10^5 \\ C_f &= \frac{0.664}{\sqrt{10^5}} = 2.099 \cdot 10^{-3} \\ \tau_w &= 2.099 \cdot 10^{-3} \cdot 0.5 \cdot 1.225 \frac{Kg}{m^3} \cdot 100 \frac{m^2}{sec^2} \approx 0.1289\ N \\ u_\tau &= \sqrt{\frac{0.1289}{1.225}} = 0.324\ \frac{m}{sec} \\ &\Downarrow \\ y = \frac{y^+ \nu}{u_\tau} &= \frac{100 \cdot 15 \cdot 10^{-6}\ \frac{m^2}{sec}}{0.324\ \frac{m}{sec}} = 4.6294 \cdot 10^{-3}\ m \end{aligned}$$

References

[1] Mohamed Gad-el Hak. Flow Control: Passive, Active, and Reactive Flow Management. Cambridge University Press, 2000.

[2] Lin Chen, Keisuke Asai, Taku Nonomura, Guannan Xi, and Tianshu Liu. A review of backward-facing step (bfs) flow mechanisms, heat transfer and control. Thermal Science and Engineering Progress, 6:194 – 216, 2018.

[3] Yuki Koide, Ryota Sasaki, Yuki Kameya, and Masahiro Motosuke. A burst wave-induced plasma actuator for controlling separated flow over a backward-facing step at low reynolds number. Experimental Thermal and Fluid Science, 66, 09 2015.

[4] David Greenblatt and Israel J. Wygnanski. The control of flow separation by periodic excitation. Progress in Aerospace Sciences, 36(7):487 – 545, 2000.

[5] HD Taylor and HH Hoadley. Application of vortex generator mixing principles to diffusers. Research Department, United Aircraft Corporation, Concluding Report No, 1948.

[6] Junhui Huang, Thomas C Corke, and Flint O Thomas. Plasma actuators for separation control of low-pressure turbine blades. AIAA journal, 44(1):51–57, 2006.

[7] Avi Seifert, David Greenblatt, and Israel J. Wygnanski. Active separation control: an overview of reynolds and mach numbers effects. Aerospace Science and Technology, 8(7):569 – 582, 2004.

[8] Louis N Cattafesta III and Mark Sheplak. Actuators for active flow control. Annual Review of Fluid Mechanics, 43:247–272, 2011.

[9] D Dolgopyat and A Seifert. Active flow control virtual maneuvering system applied to conventional airfoil. AIAA Journal, 57(1):72–89, 2018.

[10] A Seifert, S Eliahu, D Greenblatt, and I Wygnanski. Use of piezoelectric actuators for airfoil separation control. AIAA journal, 36(8):1535–1537, 1998.

[11] W-P Jeon and Ron F Blackwelder. Perturbations in the wall region using flush mounted piezoceramic actuators. Experiments in Fluids, 28(6):485–496, 2000.

[12] Eric Moreau. Airflow control by non-thermal plasma actuators. Journal of physics D: applied physics, 40(3):605, 2007.

[13] M Samimy, I Adamovich, B Webb, J Kastner, J Hileman, S Keshav, and P Palm. Development and characterization of plasma actuators for high-speed jet control. Experiments in Fluids, 37(4):577–588, 2004.

[14] Yurii G Utkin, Saurabh Keshav, Jin-Hwa Kim, Jeff Kastner, Igor V Adamovich, and Mo Samimy. Development and use of localized arc filament plasma actuators for high-speed flow control. Journal of Physics D: Applied Physics, 40(3):685, 2006.

[15] Venkateswaran Narayanaswamy, Laxminarayan L Raja, and Noel T Clemens. Characterization of a high-frequency pulsed-plasma jet actuator for supersonic flow control. AIAA journal, 48(2):297–305, 2010.

[16] Giuseppe Correale. Flow control over a backward facing step by ns-dbd plasma actuator. In 52nd Aerospace Sciences Meeting, 06 2015.

[17] Ata Esfahani, Achal Singhal, Christopher J Clifford, and Mo Samimy. Flow separation control over a boeing vertol vr-7 using ns-dbd plasma actuators. In 54th AIAA Aerospace Sciences Meeting, page 0843, 2016.

[18] Anton Ronis and Igal Kronhaus. Spatial spectroscopic analysis of a cathodic arc jet. In AIAA Scitech 2019 Forum, page 0738, 2019.

[19] Anton Ronis and Igal Kronhaus. Thrust generation of the cathodic arc in ambient air. Journal of Physics D: Applied Physics, 52(32):324004, jun 2019.

[20] Matar M. Rosen, Anton Ronis, and Igal Kronhaus. The influence of cathodic arc jet on separated subsonic flow over backward facing step, 2020 – *Submitted*.

[21] M. A. Z. Hasan. The flow over a backward-facing step under controlled perturbation: laminar separation. Journal of Fluid Mechanics, 238:73–96, 1992.

[22] Wind tunnel index. `https://www.grc.nasa.gov/www/k-12/airplane/shortt.html`. Accessed: spring 2019.

[23] J. W. Naughton, J. Robinson, and V. Durgesh. Oil-film interferometry measurement of skin friction - analysis summary and description of matlab program. In 20th International Congress on Instrumentation in Aerospace Simulation Facilities, 2003. ICIASF '03., pages 169–178, Aug 2003.